

A numerical method to compute optical conductivity based on the pump-probe simulations

Can Shao,¹ Takami Tohyama,² Hong-Gang Luo,^{1,3} and Hantao Lu^{1,*}

¹*Center for Interdisciplinary Studies & Key Laboratory for Magnetism and Magnetic Materials of the MoE, Lanzhou University, Lanzhou 730000, China*

²*Department of Applied Physics, Tokyo University of Science, Tokyo 125-8585, Japan*

³*Beijing Computational Science Research Center, Beijing 100084, China*

(Dated: November 18, 2018)

A numerical method to calculate optical conductivity based on a pump-probe setup is presented. Its validity and limits are demonstrated via the numerical simulations on the half-filled one-dimensional extended Hubbard model both in equilibrium and out of equilibrium. By employing either a step-like or a Gaussian-like probing vector potential, it is found that in nonequilibrium, the method can be related to the linear response theory or a different generalized Kubo formula, respectively. The observation reveals the probe-pulse dependence of the optical conductivity in nonequilibrium, which may have its applications in the theoretical analysis of ultrafast spectroscopy measurements.

PACS numbers: 71.27.+a, 78.47.-p

I. INTRODUCTION

Time-resolved spectroscopy has been extensively applied to investigate the dynamic properties of materials with strong correlations, e.g., on one-dimensional (1D) Mott insulators such as ET-F₂TCNQ¹⁻³ and the halogen-bridged transition-metal compounds^{4,5}, and on higher dimensional correlated systems, such as cuprates⁶⁻⁹ and manganites^{10,11}. As a promising time-resolved spectroscopy technique, the ultrafast pump-probe optical measurements are able to disentangle the complicated entanglement of various degrees of freedom within the systems to some extent by resolving their contributions separately at multiple time scales¹². For electronic systems, the time-dependent optical conductivity is a typical measurement, from which the related dynamic information can be extracted.

Theoretically, there are various ways to investigate the nonequilibrium dynamic response in correlated systems. One is based on the nonequilibrium Green's functions. By using the Kadanoff-Baym or Keldysh formalism, methods which have been applied to correlated systems in equilibrium, such as the dynamic mean-field theory, can be adapted to nonequilibrium on a formal level (see, e.g., Ref. 13 and references there). Another way starts from the wave functions, which is primarily employed to closed systems. The time-dependent wave functions are secured by various numerical methods, such as the exact diagonalization and the density-matrix renormalization group, thereafter the expectation values of observables as functions of time can then be readily obtained, enabling further calculations on the out-of-equilibrium dynamic response. When the time-dependent optical conductivity is concerned, several related yet different schemes have been used, including the nonequilibrium generalizations of the Kubo formula¹⁴ and linear response theory^{15,16}, which will be discussed later.

In this paper, inspired by the pump-probe experimental setup, we propose a method to calculate the optical conductivity. Its validity and limits are demonstrated by the detailed numerical simulations on the 1D half-filled extended Hubbard model, a prototype of strongly correlated electronic systems. A comparison study between our method and the existing ones in both equilibrium and out of equilibrium cases is made. We find that by adopting two different limits on the probe pulse, our method can reproduce the results of the generalized Kubo formula and the linear response theory. The theoretical analysis combined with numerical simulations elucidates the difference and connections between these various methods to a satisfactory level.

The rest of the paper is organized as follows. In Sec. II, after the model description and a critical review on relevant existing methods, our approach is presented. The following section gives a theoretical analysis on the validity of the approach, with a numerical demonstration concerning the options for probe-pulse parameters. In Sec. IV, comprehensive comparisons and analysis are made. The conclusion is given in Sec. V.

II. MODEL AND METHODS

The Hamiltonian we discuss is the well-known 1D extended Hubbard model at half-filling:

$$\begin{aligned} H = & -t_h \sum_{i,\sigma} \left(c_{i,\sigma}^\dagger c_{i+1,\sigma} + \text{H.c.} \right) \\ & + U \sum_i \left(n_{i,\uparrow} - \frac{1}{2} \right) \left(n_{i,\downarrow} - \frac{1}{2} \right) \\ & + V \sum_i (n_i - 1) (n_{i+1} - 1), \end{aligned} \quad (1)$$

where $c_{i,\sigma}^\dagger$ ($c_{i,\sigma}$) is creation (annihilation) operator of electron with spin σ at site i , $n_{i,\sigma} = c_{i,\sigma}^\dagger c_{i,\sigma}$, $n_i = n_{i,\uparrow} + n_{i,\downarrow}$, t_h is the hopping constant, U and V are on-site and nearest-neighbor Coulomb repulsion interactions, respectively. In the following, we set t_h and t_h^{-1} as energy and time units and take Plank constant $\hbar = 1$, and the elementary charge $e = 1$.

We restrict our discussions to zero temperature since the results there are most transparent. Before introducing our method in detail, we first present some existing relevant methods.

It is well known that the optical conductivity in equilibrium can be calculated by the Kubo formula in the linear response regime. The regular part of the optical conductivity (excluding the possible singularity at $\omega = 0$) in general is given by the current-current correlation function as:

$$\begin{aligned} \text{Re } \sigma_{\text{reg}}(\omega) &= -\frac{1}{\omega L} \lim_{\delta \rightarrow 0^+} \text{Im } \chi(\omega + i\delta) \\ &= \frac{\pi}{L} \sum_{n \neq 0} \frac{1}{E_{n0}} |\langle 0 | j | n \rangle|^2 [\delta(\omega - E_{n0}) + \delta(\omega + E_{n0})], \end{aligned} \quad (2)$$

where $E_{n0} := E_n - E_0$, L is the number of lattice, and

$$\chi(\omega) = \int_{-\infty}^{+\infty} ds e^{i\omega s} (-i)\theta(s) \langle 0 | [j(s), j(0)] | 0 \rangle. \quad (3)$$

$j(t)$ in Eq. (3) is the Heisenberg representation of the current operator j , which reads

$$j = -it_h \sum [c_{i,\sigma}^\dagger c_{i+1,\sigma} - \text{H.c.}]. \quad (4)$$

For convenience, we give this Kubo formula method an abbreviation as KF.

On the other hand, in nonequilibrium when the time translation invariance does not hold in general, a two-time optical conductivity $\sigma(t', t)$ is required in order to describe the linear response of the electrical current to a time-dependent probing field $\delta \mathbf{E}(t)$ ¹⁷:

$$\delta \langle \mathbf{j}(t') \rangle = \int_{-\infty}^{t'} dt \sigma(t', t) \delta \mathbf{E}(t). \quad (5)$$

The partial Fourier transformation on the real-time conductivity follows the definition in Ref. 16

$$\sigma(\omega, t) = \int_0^{t_m} ds \sigma(t+s, t) e^{i(\omega + i\eta)s}, \quad (6)$$

where a spectral broadening factor η and the window width t_m for the Fourier transformation, which are used in the numerical simulations, are also introduced explicitly. According to the definition, $\sigma(\omega, t)$ measures the *causal* response of the system at a given probing time t .

The Kubo formula in equilibrium (Eq. (2)) can be formally generalized to nonequilibrium cases and has been used quite often in the literature¹⁴:

$$\begin{aligned} \text{Re } \sigma_{\text{reg}}(\omega, t) &= \frac{1}{\omega L} \text{Im} \int_0^{t_m} ds [ie^{i(\omega + i\eta)s} \times \\ &\quad \langle \psi(t) | [j^I(t+s), j^I(t)] | \psi(t) \rangle]. \end{aligned} \quad (7)$$

Here the interaction representation operator $B^I(t')$ is defined as $U^\dagger(t', t) B U(t', t)$, where $U(t', t)$ is the time-evolution operator *without probing perturbations*¹⁶. We call this nonequilibrium generalization of the Kubo formula as NKF in the paper.

Another nonequilibrium formula is based on more rigorous analysis of linear response theory^{15,16}, and $\sigma(t', t)$ (with restriction $t' \geq t$) is given by

$$\sigma(t', t) = \frac{1}{L} \left[\langle \psi(t') | \tau | \psi(t') \rangle + \int_t^{t'} dt'' \chi(t', t'') \right], \quad (8)$$

where

$$\chi(t', t'') = -i\theta(t' - t'') \langle \psi(t) | [j^I(t'), j^I(t'')] | \psi(t) \rangle, \quad (9)$$

and $\tau = t \sum_{i,\sigma} (c_{i+1,\sigma}^\dagger c_{i,\sigma} + \text{H.c.})$, which is the stress tensor operator. We name this nonequilibrium linear response theory as NLR in the paper.

We notice that the link between NKF and NLR can be established by a variant of Eq. (8), which is defined by:

$$\sigma(t', t) = \frac{1}{L} \left[\langle \psi(t') | \tau | \psi(t') \rangle + \int_t^{t'} dt'' \chi(t'', t) \right], \quad (10)$$

where

$$\chi(t'', t) = -i\theta(t'' - t) \langle \psi(t) | [j^I(t''), j^I(t)] | \psi(t) \rangle. \quad (11)$$

Regarding Eq. (10) as a variant of NLR, we call it VNLR. It is also easy to recognize that VNLR has a close relation to NKF, since Eq. (7) is just the real regular part of the Fourier transformation on t' for the second term in Eq. (10). Actually the difference between NLR and VNLR comes from the second term in Eqs. (8) and (10), where under the integration over the intermediate moment $t'' \in (t, t')$, the two-time commutators of the current operator take place at t'' to t' , and t to t'' , respectively (see Eq. (9) and Eq. (11)). Note that t and t' are the starting time and ending time of the two-time optical conductivity $\sigma(t', t)$ with $t' \geq t$, respectively. The above description is illustrated in Fig. 1.

A few more words on NLR and VNLR could be helpful. We argue that the NLR method, which is derived more rigorously from the linear response theory¹⁶, contains more complete information of the time correlations than VNLR (or equivalently for NKF). It can be easily apprehended from Fig. 1, reminding that $\sigma(\omega, t)$ is the Fourier transformation of $\sigma(t', t)$ with respect to t' . The fact suggests that the VNLR is a kind of partial time correlation average of the NLR. On the other hand, for the equilibrium case, the two methods coincide completely due to the time translation invariance. The ramification of the partial summation of the full time correlations will be discussed in more detail in Sec. IV.

After the brief review and analysis on the relevant existing methods, we now move to our method. Inspired by the experimental pump-probe setup and the theoretical

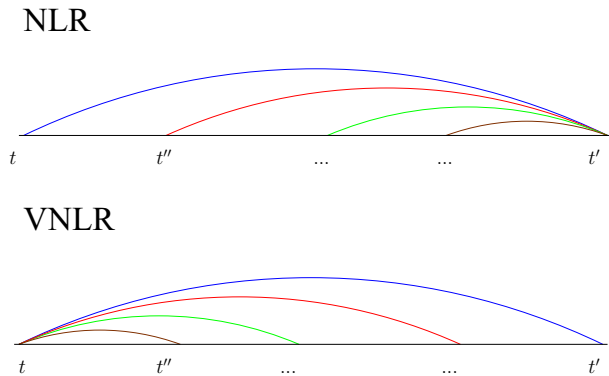


FIG. 1. (Color online) A schematic diagram of the current-current correlations considered in NLR and VNLR, respectively.

works on coherent dynamics of the BCS model^{18,19}, we propose a method to calculate the optical conductivity of the Hubbard model in both equilibrium and out of equilibrium as follows.

First, one notes that an *external* electric field applied to the Hamiltonian (1) can be incorporated via the Peierls substitution in the hopping terms as:

$$c_{i,\sigma}^\dagger c_{i+1,\sigma} \rightarrow e^{iA(t)} c_{i,\sigma}^\dagger c_{i+1,\sigma}, \quad H \rightarrow H(t). \quad (12)$$

In equilibrium, we set the vector potential $A(t)$ to be a weak probe pulse denoted as $A_{\text{probe}}(t)$. The detail forms of the probe pulse will be discussed later. With the knowledge of the wave function $\psi(t)$ under the action of $A_{\text{probe}}(t)$, we can obtain the temporal evolution of the expectation value of the current operator $\langle j(t) \rangle$, which is defined as $\langle j(t) \rangle = \langle \psi(t) | j | \psi(t) \rangle$. Note that with the existence of $A(t)$, the current operator j becomes

$$j = \frac{\delta H(t)}{\delta A(t)} = -it_h \sum [e^{iA(t)} c_{i,\sigma}^\dagger c_{i+1,\sigma} - \text{H.c.}]. \quad (13)$$

For clarity, we denote the current part induced by the probe pulse as $\langle j_{\text{probe}}(t) \rangle$. The optical conductivity can then be evaluated by

$$\sigma(\omega) = \frac{j_{\text{probe}}(\omega)}{i(\omega + i\eta)LA_{\text{probe}}(\omega)}, \quad (14)$$

where $j_{\text{probe}}(\omega)$ and $A_{\text{probe}}(\omega)$ are the Fourier transformations of $\langle j_{\text{probe}}(t) \rangle$ and $A_{\text{probe}}(t)$, respectively. Note that numerically, a damping factor $e^{-\eta}$ is also introduced in the Fourier transformations, same as the above two methods. And the same η in the denominator of Eq. (14) is necessary for obtaining the spectral weight that is due to the Drude peak in the limit of $\omega \rightarrow 0$, which will be discussed later in more detail in Sec. IV.

We are ready to extend the algorithm to nonequilibrium, which can be driven either by a pump pulse or a quench. The key is that in order to identify the response

of the system with respect to the later probe pulse, a subtraction is necessary, i.e., two steps are involved (each step follows similar process described above) in order to calculate the optical conductivity in nonequilibrium²⁰. First, a time-evolution process in the absence of probe pulse is evaluated and we obtain $\langle j(t) \rangle$. Secondly, in the presence of a probe pulse, we get $\langle j_{\text{total}}(t) \rangle$. The subtraction of $\langle j(t) \rangle$ from $\langle j_{\text{total}}(t) \rangle$ produces the required $\langle j_{\text{probe}}(t) \rangle$. Then the optical conductivity in nonequilibrium is

$$\sigma(\omega, t_{\text{probe}}) = \frac{j_{\text{probe}}(\omega, t_{\text{probe}})}{i(\omega + i\eta)LA_{\text{probe}}(\omega)}, \quad (15)$$

where t_{probe} is the probing time. The abbreviation for this pump-probe-based method is PP.

Finally, in order to trace the temporal evolution of the system, we employ the time-dependent Lanczos method to evaluate $|\psi(t)\rangle$ as²¹:

$$|\psi(t + \delta t)\rangle \simeq \sum_{l=1}^M e^{-i\epsilon_l \delta t} |\phi_l\rangle \langle \phi_l | \psi(t)\rangle, \quad (16)$$

where ϵ_l and $|\phi_l\rangle$, respectively, are eigenvalues and eigenvectors of the tridiagonal matrix generated in the Lanczos iteration. M is the dimension of the Lanczos basis and δt is the minimum time step.

III. THE INFLUENCE OF THE PROBE PULSES - A THEORETICAL ARGUMENT

In the PP method, analogous to experiments, it is important that the strength of the probe pulse should be weak enough to prevent disturbing the system's dynamics qualitatively. Meanwhile, the influence of the forms of the probe pulse is also crucial. The point can be made clear in the following argument.

We begin with the specific form of Eq. (5) in 1D:

$$\langle j_{\text{probe}}(t') \rangle = \int_{t_0}^{t'} \sigma(t', t'') E_{\text{probe}}(t'') dt'', \quad (17)$$

where we have assumed that the probe electric field is turned on after t_0 , and $t' > t_0$. The Fourier transformation on $\langle j_{\text{probe}}(t') \rangle$ gives

$$\begin{aligned} j_{\text{probe}}(\omega) &= \int_{t_0}^{t_M} dt' \langle j_{\text{probe}}(t') \rangle e^{i\omega t'} \\ &= \int_{t_0}^{t_M} dt' \int_{t_0}^{t'} dt'' \sigma(t', t'') E_{\text{probe}}(t'') e^{i\omega t'} \\ &= \int_{t_0}^{t_M} dt'' \int_{t''}^{t_M} dt' \sigma(t', t'') E_{\text{probe}}(t'') e^{i\omega(t' - t'')} e^{i\omega t''} \\ &= \int_{t_0}^{t_M} dt'' \sigma(\omega, t'') E_{\text{probe}}(t'') e^{i\omega t''}, \end{aligned} \quad (18)$$

where t_M is the maximum evolution time and $t_M \gg t_0$. We can see that in order to obtain $\sigma(\omega, t)$ (assuming $t \in$

(t_0, t_M) . In this section for notational convenience we mark t as the probing time), the most convenient choice of E_{probe} in theory is a δ -pulse as $E_{\text{probe}}(t'') \sim \delta(t'' - t)$. In the temporal gauge, it corresponds to a step-like vector potential, i.e., $A_{\text{probe}}(t'') = A_{0,\text{step}} \theta(t'' - t)$, where $\theta(t'')$ is the Heaviside step function. We call this kind of PP method with a step-like vector potential as the PP-step. From Eq. (18) it is easy to verify that Eq. (15) is exact under the step potential.

However, for more realistic approaches to ultrafast spectroscopy measurements, instead of using the δ -pulse, the probe pulse can be simulated by^{22,23}

$$A_{\text{probe}}(t'') = A_{0,\text{probe}} e^{-(t''-t)^2/2t_{d,\text{probe}}^2} \times \cos[\omega_{\text{probe}}(t'' - t)], \quad (19)$$

where a Gaussian-like envelope around t is used with $t_{d,\text{probe}}$ characterizing the temporal width of the probe pulse, and ω_{probe} is the central frequency. Following the previous conventions, the PP method with the Gaussian-like vector potential is called PP-Gaussian. It is important to note that in the PP-Gaussian, unlike the PP-step, $A_{\text{probe}}(t'') \rightarrow 0$ as $t'' \rightarrow \pm\infty$, and usually, the electric field satisfies $\int_{t_i}^{t_f} E(t'') dt'' \approx \int_{-\infty}^{+\infty} E(t'') dt'' = 0$, which is the general case in the experimental situations²⁴.

Let us examine what approximations have been made in order to reach Eq. (15) in the PP-Gaussian. Suppose that the pulse being activated during $[t, t + \Delta t]$, i.e., $E_{\text{probe}}(t'') \neq 0$ only when $t'' \in [t, t + \Delta t]$, and consequently, $\langle j_{\text{probe}}(t') \rangle = 0$ when $t' < t$ in Eq. (17), we have

$$j_{\text{probe}}(\omega) = \int_t^{t+\Delta t} dt'' \sigma(\omega, t'') E_{\text{probe}}(t'') e^{i\omega t''} \approx \sigma(\omega, t) E_{\text{probe}}(\omega). \quad (20)$$

The key approximation in Eq. (20) is the last step, where $\sigma(\omega, t'')$ is approached by $\sigma(\omega, t)$ and moved to the outside of the integration, and thus somehow Eq. (15) can be justified. The validity of the approximation requires a narrow probe pulse, i.e., $t_{d,\text{probe}}$ should be small enough. A numerical check on the influence of $t_{d,\text{probe}}$ is shown in Fig. 2, where the zero-temperature optical conductivity $\sigma(\omega)$ for the Hamiltonian (1) on the $L = 10$ lattice is calculated by the PP-Gaussian with different values of $t_{d,\text{probe}}$. It shows that when $t_{d,\text{probe}} \leq 0.2$, the results are actually converged. It is also noted that by adopting a narrow probe pulse with small enough $t_{d,\text{probe}}$, central frequency of the pulse ω_{probe} can be chosen rather freely, since due to finite t_d , the incoming photon frequency is broadened into a Gaussian-like distribution, with the variance of $1/t_d^2$ around ω_{probe} .

The above arguments seem to suggest that with small enough $t_{d,\text{probe}}$, the results of the PP-Gaussian and PP-step would coincide. However there is a critical difference between them. In the PP-Gaussian, the induced current $\langle j_{\text{probe}}(t') \rangle$, as shown in Eq. (17), is just produced by the highly temporally localized perturbation in the range of $[t, t + \Delta t]$ (outside of the range, *both* the electric field and

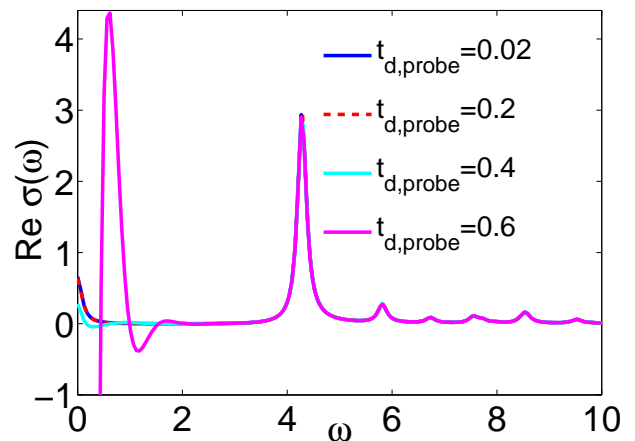


FIG. 2. (Color online) The calculated $\text{Re} \sigma(\omega)$ in equilibrium (zero temperature) for the Hamiltonian (1) with different $t_{d,\text{probe}}$ by the PP-Gaussian method. Parameters: $L = 10$, $U = 10$, $V = 4.5$, $\omega_{\text{probe}} = 10$, and $A_{0,\text{probe}} = 1.0 \times 10^{-6}$.

the vector potential are practically zero). Consequently, it is reasonable to suggest that when the Gaussian-like pulse is used, only the correlations between the variant t' and (roughly) fixed t are taken into account in the calculation of $\sigma(\omega, t)$. On the other hand, the linear response theory requires, as clearly demonstrated in Eqs. (8) and (9), a persistent perturbation (with the form as $\sim j \cdot A$) during $[t', t]$, which is indeed fulfilled by a step-like vector potential in the PP-step (although the electric field is a temporal δ -function with the singularity at t). From the above analysis, we thus propose that the PP-step and PP-Gaussian can be identified with the NLR and VNLN, respectively. The proposition will be examined in the next section numerically.

In our following simulations, we set $M = 30$, $\delta t = 0.02$, $\eta = 1/L$, and $L = 10$. For the PP-step, $A_{0,\text{step}} = 1.0 \times 10^{-4}$; for the PP-Gaussian, $A_{0,\text{probe}} \sim 10^{-6}$, $t_{d,\text{probe}} = 0.02$, and $\omega_{\text{probe}} = 10$. Only the real parts of the optical conductivity are displayed. In despite of double temporal evolutions being involved, our method is faster and less memory-demanding than NKF or (V)NLR because no integration is required¹⁶.

IV. RESULTS AND COMPARISON

In this section, working on the 1D half-filled extended Hubbard model (1), we compare the numerical results of the optical conductivity both in equilibrium and out of equilibrium between various methods.

We first discuss the equilibrium case. Figure 3 shows the results in equilibrium under the open and periodic boundary conditions (BCs), obtained by three methods, i.e., KF, NLR and PP. Note that as a generalization of the KF method to nonequilibrium, the NKF produces identical results with the KF in equilibrium, and there is also no difference between the results from the PP-step

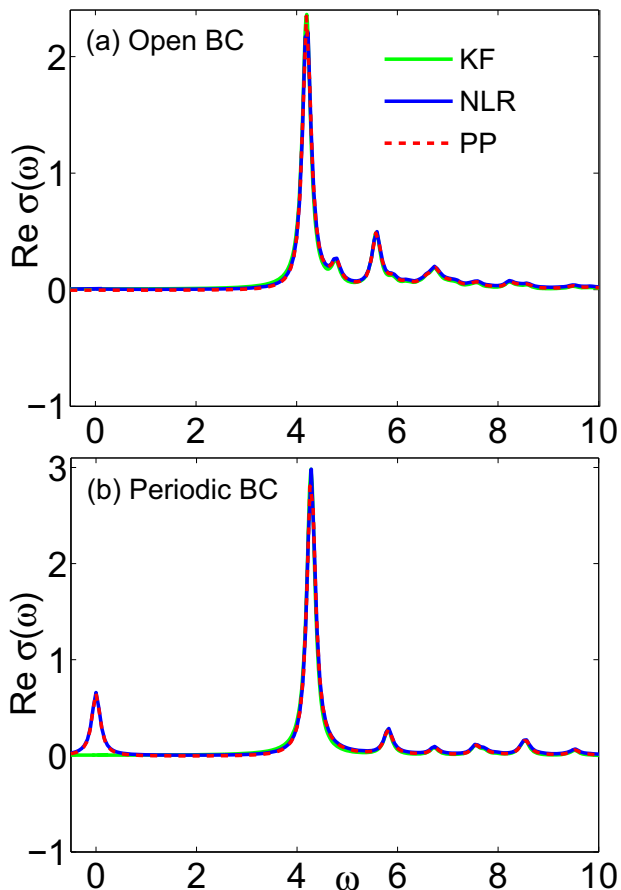


FIG. 3. (Color online) $\text{Re } \sigma(\omega)$ in equilibrium (zero temperature) obtained by the KF, NLR, and PP methods in (a) the open boundary condition (open BC) and (b) periodic BC. Parameters: $L = 10$, $U = 10$, $V = 4.5$.

and PP-Gaussian. We can see that the results obtained by the three methods coincide well except in the vicinity of $\omega = 0$ in the periodic BC. In Fig. 3(b), an identical peak around zero frequency is produced both by the PP and NLR, while it is absent in the result of the KF. The small peak is known to originate from the nonzero charge stiffness (Drude weight) in the periodic BC for *finite systems*, even when the system is in an insulating phase. The reason is following. The charge stiffness D is related to the singularity at $\omega = 0$ in the real part of the conductivity as^{25,26}:

$$\text{Re } \sigma(\omega) = 2\pi D \delta(\omega) + \text{Re } \sigma_{\text{reg}}(\omega), \quad (21)$$

and here

$$D = (1/2L)[\langle \tau \rangle + \text{Re } \chi(\omega = 0)], \quad (22)$$

where $\chi(\omega)$ is defined in Eq. (3). We can see that the Drude weight component comes from the net contribution of the diamagnetic term ($\langle \tau \rangle$) and the current-current correlations at $\omega = 0$. For an insulator, though D should vanish in the thermodynamic limit, it might

remain finite when the system size is finite. It has been confirmed by the sum rule check (not shown here) that for our model at half filling with $L = 10$, D has a sizable value in the periodic BC, while in the open BC the value is negligible. The introduction of the η factor in the numerical calculations renders the singularity at $\omega = 0$ (the δ -function) into a small peak, as shown in Fig. 3(b). We can see here that the Drude weight contribution to the conductivity can be captured both by the NLR and PP methods, while the KF method, which only takes into account the regular part of the current-current correlations as shown in Eq. (2), fails to produce this feature.

We are ready to move to the nonequilibrium cases and here three well-attended setups are considered. First, the external field is a pump pulse with the form similar to Eq. (19) (formally just replace "probe" with "pump"), and we call this situation as Pump case. Secondly, a temporary δ -like electric pulse can be simulated by introducing a phase shift $e^{i\theta}$ in the hopping terms of Eq. (1) at $t = 0$, similar to Eq. (12). The strength of the pulse is controlled by θ . In our calculations we choose $\theta = \pi$, an extreme case and known as π -quench. The third situation is called U -quench, where the value of U changes at $t = 0$. This situation can be realized, for example, in cold atoms²⁷.

Figure 4 shows the results of $\text{Re } \sigma(\omega, t)$ at $t = 10$ for these three situations obtained by different methods. First note that the NKF method only includes the regular part of the current-current correlation term (see Eq. (7)). As a result, $\text{Re } \sigma(\omega, t)$ equals to zero at $\omega = 0$ exactly. Away from the vicinity of $\omega = 0$, the results of NKF and VNLR are consistent. This is not surprising since the NKF is just about the regular part of VNLR. More importantly, from Fig. 4, we can see that in all these three cases including pump and quench, the results between PP-Gaussian and VNLR (left column), PP-step and NLR (right column) coincide well with each other, verifying the proposition in Sec. III of the equivalence among these groups. Thus we make it clear that the NKF and NLR, as being widely used in the dynamic response study, actually correspond to two different limits of probe, which has either a Gaussian-like vector potential with a vanishing width, or a step-like one. The former with a tiny width as small as $t_{\text{d,probe}} = 0.02$ actually can be regarded as an approximation of the temporal delta-like potential, which has been numerically confirmed in our calculations (not shown here). Though the electric fields are both highly temporally confined in these two cases, one essential difference is the persistency (or temporal locality in the opposite sense) of the vector potential in the subsequent time evolutions, which results in the (non)vanishing of the time integral of the electric field over the probing time. It suggests that the time-dependent conductivity, or other similar transport quantities measured in nonequilibrium, may depend on the details of probe, and the theoretical investigations should take into account the relevant experimental setup sufficiently.

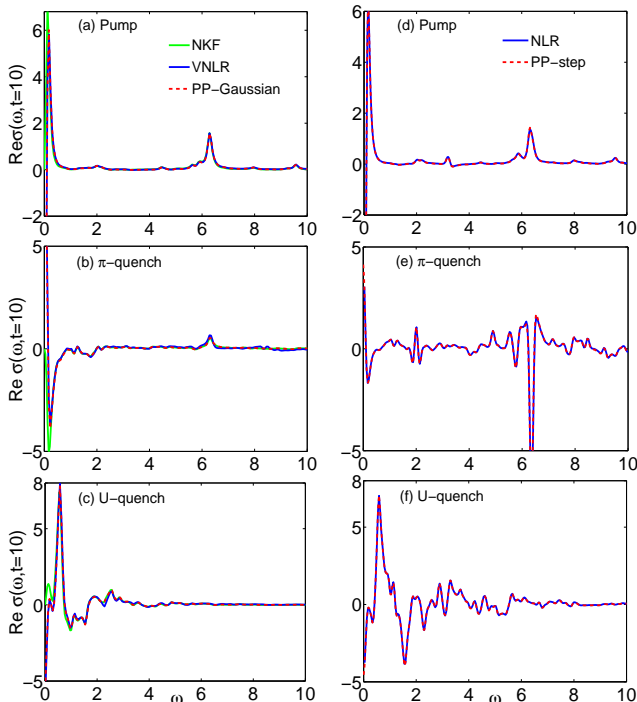


FIG. 4. (Color online) The time-dependent optical conductivity $\text{Re}\sigma(\omega, t)$ at $t = 10$ obtained by different methods in the periodic BC, where t is the time delay relative to the pump pulse or quench. In (a) and (d), a pump pulse is applied with parameters $A_{0,\text{pump}} = 0.2$, $\omega_{\text{pump}} = 6.29$ (resonant frequency), and $t_{d,\text{pump}} = 0.5$. In (b) and (e), a π -quench is applied. In (c) and (f), a U -quench with the value of U changed from 10 to 4 is applied. The blue solid lines represent the results of the VNLR and NLR in the left ((a), (b), and (c)) and right ((d), (e), and (f)) columns, respectively, while the red dashed lines represent the results of the PP-Gaussian and PP-step in different columns. Model parameters: $L = 10$, $U = 10$, $V = 3$.

Additionally, as shown in Fig. 4, similar development of $\sigma(\omega, t)$ between the left and right columns can still be recognized regardless of the notable difference in quenches. This is consistent with the previous statement in Sec. II that the VNLR is a kind of average on NLR by a partial summation of the full time correlations. In the Pump case, the results of VNLR and NLR are more close

to each other²⁰, which might be due to the fact that, we suspect, the Hamiltonian only changes temporarily due to the applying pump pulse and after that it goes back; while in both π -quench and U -quench, the Hamiltonian undergoes an essential change after the quench time.

V. CONCLUSION

In this paper, we introduce a numerical method to calculate the time-dependent optical conductivity based on the simulation of the pump-probe experimental setup. According to the property of the probe pulse, two different approaches are discussed, i.e., PP-step and PP-Gaussian, using either a step-like or a Gaussian-like probing vector potential. We find that the two approaches can be identified with the nonequilibrium linear response theory and one of its variants, respectively. Thus the connections between these various methods and their differences are clarified. A numerical verification is given by employing the method systematically to the 1D half-filled extended Hubbard model, both in equilibrium and out of equilibrium. The later includes three well-attended cases: the Pump, π -quench and U -quench. In the numerical results, the probe-pulse dependence of the optical conductivity in nonequilibrium is especially significant in the quenches. We suggest that such difference might be able to be observed if the two kinds of probe pulse can be arranged in these experiments.

ACKNOWLEDGMENTS

The authors thank Janez Bonča, Denis Golež and Dirk Manske for helpful discussions. H.L. acknowledges support from the National Natural Science Foundation of China (NSFC) (Grants Nos. 11325417, 11474136, and 11174115), and the open project of State Key Laboratory of Theoretical Physics (SKLTP) in ITP, CAS. T.T. acknowledges support by the Grant-in-Aid for Scientific Research (26287079) from MEXT and the Strategic Programs for Innovative Research (SPIRE) (hp140215, hp150211), the Computational Materials Science Initiative (CMSI).

* luht@lzu.edu.cn

¹ H. Okamoto, H. Matsuzaki, T. Wakabayashi, Y. Takahashi, and T. Hasegawa, Phys. Rev. Lett. **98**, 037401 (2007).

² S. Wall, D. Brida, S. R. Clark, H. P. Ehrke1, D. Jaksch, A. Ardavan, S. Bonora, H. Uemura, Y. Takahashi, T. Hasegawa, H. Okamoto, G. Cerullo, and A. Cavalleri, Nature Phys. **7**, 114 (2011).

³ M. Mitrano, G. Cotugno, S.R. Clark, R. Singla, S. Kaiser, J. Stähler, R. Beyer, M. Dressel, L. Baldassarre, D. Nicoletti, A. Perucchi, T. Hasegawa, H. Okamoto, D. Jaksch,

and A. Cavalleri, Phys. Rev. Lett. **112**, 117801 (2014).

⁴ S. Iwai, M. Ono, A. Maeda, H. Matsuzaki, H. Kishida, H. Okamoto, and Y. Tokura, Phys. Rev. Lett. **91**, 057401 (2003).

⁵ H. Matsuzaki, M. Iwata, T. Miyamoto, T. Terashige, K. Iwano, S. Takaishi, M. Takamura, S. Kumagai, M. Yamashita, R. Takahashi, Y. Wakabayashi, and H. Okamoto, Phys. Rev. Lett. **113**, 096403 (2014).

⁶ D. Fausti, R. I. Tobey, N. Dean, S. Kaiser, A. Dienst, M. C. Hoffmann, S. Pyon, T. Takayama, H. Takagi, and A. Cavalleri, Science **331**, 189 (2011).

- ⁷ D. Nicoletti, E. Casandruc, Y. Laplace, V. Khanna, C. R. Hunt, S. Kaiser, S. S. Dhesi, G. D. Gu, J. P. Hill, and A. Cavalleri, *Phys. Rev. B* **90**, 100503(R) (2014).
- ⁸ W. Hu, S. Kaiser, D. Nicoletti, C. R. Hunt, I. Gierz, M. C. Hoffmann, M. Le Tacon, T. Loew, B. Keimer, and A. Cavalleri, *Nature Mater.* **13**, 705 (2014).
- ⁹ S. Dal Conte, L. Vidmar, D. Golež, M. Mierzejewski, G. Soavi, S. Peli, F. Banfi, G. Ferrini, R. Comin, B. M. Ludbrook, L. Chauviere, N. D. Zhigadlo, H. Eisaki, M. Greven, S. Lupi, A. Damascelli, D. Brida, M. Capone, J. Bonča, G. Cerullo, and C. Giannetti, *Nature Phys.* **11**, 421-426 (2015).
- ¹⁰ Matteo Rini, Ra'anan Tobey, Nicky Dean, Jiro Itatani, Yasuhide Tomioka, Yoshinori Tokura, Robert W. Schoenlein, and Andrea Cavalleri, *Nature* **449**, 72-74 (2007).
- ¹¹ Tianqi Li, Aaron Patz, Leonidas Mouchliadis, Jiaqiang Yan, Thomas A. Lograsso, Ilias E. Perakis, and Jigang Wang, *Nature* **496**, 69-73 (2013).
- ¹² J. Orenstein, *Phys. Today* **65**, 44 (2012).
- ¹³ H. Aoki, N. Tsuji, M. Eckstein, M. Kollar, T. Oka, and P. Werner, *Rev. Mod. Phys.* **86**, 779 (2014).
- ¹⁴ G. De Filippis, V. Cataudella, E. A. Nowadnick, T. P. Devereaux, A. S. Mishchenko, and N. Nagaosa, *Phys. Rev. Lett.* **109**, 176402 (2012).
- ¹⁵ Davide Rossini, Rosario Fazio, Vittorio Giovannetti, and Alessandro Silva, *Europhys. Lett.* **107**, 30002 (2014).
- ¹⁶ Z. Lenarčič, D. Golež, J. Bonča, and P. Prelovšek, *Phys. Rev. B* **89**, 125123 (2014).
- ¹⁷ Martin Eckstein, Marcus Kollar, and Philipp Werner, *Phys. Rev. B* **81**, 115131 (2010).
- ¹⁸ T. Papenkort, V. M. Axt, and T. Kuhn, *Phys. Rev. B* **76**, 224522 (2007).
- ¹⁹ Andreas P. Schnyder, Dirk Manske, and Adolfo Avella, *Phys. Rev. B* **84**, 214513 (2011).
- ²⁰ Hantao Lu, Can Shao, Janez Bonča, Dirk Manske, and Takami Tohyama, *Phys. Rev. B* **91**, 245117 (2015).
- ²¹ P. Prelovšek and J. Bonča, in *Strongly Correlated Systems-Numerical Methods*, edited by A. Avella and F. Mancini, Springer Series in Solid-State Sciences, Vol. 176 (Springer, Berlin, 2013), pp. 1-30.
- ²² Hantao Lu, Shigetoshi Sota, Hiroaki Matsueda, Janez Bonča, and Takami Tohyama, *Phys. Rev. Lett.* **109**, 197401 (2012).
- ²³ Julián Rincón, K. A. Al-Hassanieh, Adrian E. Feiguin, and Elbio Dagotto, *Phys. Rev. B* **90**, 155112 (2014).
- ²⁴ Lars Bojer Madsen, *Phys. Rev. A* **65**, 053417 (2002).
- ²⁵ H. Castella, X. Zotos, and P. Prelovšek, *Phys. Rev. Lett.* **74**, 972 (1995).
- ²⁶ X. Zotos and P. Prelovšek, *Phys. Rev. B* **53**, 983 (1996).
- ²⁷ Immanuel Bloch, Jean Dalibard, and Wilhelm Zwerger, *Rev. Mod. Phys.* **80**, 885 (2008).